Journal of Engineering Sciences, Assiut University, Vol. 40, No 5, pp.1359-1374 - September 2012.

AERODYNAMNIC ANALAYSIS OF A BUS MODEL

B. S. Ibrahim, M. T. Niazy, A. M. El-Rashidy, M. A. Abousetta, A. E. ElSeoudi and Y. S. Fangary

Mechanical Power Engineering Department, Faculty of Engineering, Ain Shams University Cairo, Egypt

(Received April 22, 2012 Accepted May 15, 2012)

ABSTRACT

Many research works had been carried out to study the aerodynamic behavior of different ground vehicles in order to enhance their stability and determine the aerodynamic forces acting on them. The present work focused on studying the aerodynamics of a bus model that resembles actual working buses. The study considered the pressure distribution around the bus model and determination of lift and drag forces acting. Two cases were considered; straight orientation of the bus model (i.e. parallel to the air stream) and when the bus model was yawed by an angle of 10˚ to the direction of air stream.

KEYWORDS: *Bus aerodynamics, wind tunnel tests, lift, Drag, side force.*

NOMENCLATURE

A	Frontal Projected Area of the Bus Model, m^2
A_L	Lateral Surface Area of the Bus Model, m^2
A_U	Upper or Lower Surface Area of the Bus Model, m^2
C_D	Total Drag Coefficient, -
C_{DD}	Total Drag Coefficient Measured by Force Dynamometer, -
C_{DF}	Friction Drag Coefficient, -
C_{DM}	Total Drag Coefficient Measured by Pressure Measurements, -
C_{DP}	Form Drag Coefficient, -
C_L	Lift Coefficient, -
C_P	Coefficient of Pressure, -
D_T	Total Drag Force, N
P	Pressure, Pa
P_O	Free Stream (Reference) Pressure, Pa
V	Free Stream Velocity, m/s
x/L	Dimensionless Horizontal Distance From the Origin Point
z/H	Dimensionless Vertical Distance from the Origin Point
θ	Angle Between the Flow and the Area Vector, Degree

1. INTRODUCTION

Many works have investigated ways in order to enhance aerodynamic properties of bodies and vehicles. This enhancement aimed to decrease drag force reduce power and fuel consumption. Such ways have been illustrated in works like those of Hwang and Yang [1], Anderson and Szewczyk [2], Rathakrishnan [3], Unal and Rockwell [4],

Apelt et al. [5] and Kwon and Choi [6]. Another force to be considered is the lift force. In cars, buses and trains it is required to minimize its value in order to increase their stability on the ground, while for aero-planes, increasing lift is required. This can be shown in the works of Hemida and Krajnovic [7], Cheli et al. [8] and Sterling et al. [9]. Other works have focused on the effect of crosswind which results in side forces, turning moments and yawing moments. Normally these forces and moments are required to be decreased which was investigated in works as that of Cheli et al. [8], Sterling et al. [9], Baker and Reynolds [10], Chiu [11], Chiu and Squire [12], Copley [13], Suzuki et al. [14], and Hoppmann et al. [15].

Some methods of drag reduction for bodies were proposed by changing the profile of these bodies, attaching after-bodies or splitter plates [7], [8], [16], [17] and [18].

In order to enhance aerodynamic properties for actual working vehicle, full studies of flow behavior around the designated vehicle must be conducted. Unfortunately very few papers have been issued in this field except for some studies as those of Allam et al. [19] and Cheli et al. [8].

In the present work, analysis of the aerodynamic properties of a bus model was carried out in order to understand its aerodynamic features. This study will be on a scaled bus model which resembles local buses that actually work in Egypt.

The main aim of the present work is to investigate the flow behavior over the model and to calculate the lift and drag coefficients using pressure measurements and using a drag force dynamometer. The obtained results are to introduce an integrated picture of the flow and aerodynamic effects on the bus model for a range of different values of Reynolds numbers.

2. EXPERIMENTAL PROCEDURE

The behavior and the properties of the flow were studied at two positions simulating two working conditions; the first is at zero yawing angle simulating a straight forward path of the bus model and the second position was with a yawing angle chosen to be 10˚ simulating rotation of the bus model or crosswind acting on it.

In Fig. (1) the layout of the bus is shown. It has an overall width of 90 mm, an overall height of 99 mm (excluding the tires) and an overall length of 350 mm. The origin point of the used coordinate system and the positions of pressure taps used to measure the static pressure on the bus surface are also shown.

It is considered that all sides of the model have the actual scaled details of a real bus (windows, doors, steps, etc). The only side that does not have the actual scaled details is the bottom side because the actual details are complex to be simulated and also for experimental reasons of fixation.

Aerodynamic experiments were carried out in an open circuit wind tunnel with a test section of dimensions of 300×300×500 mm and the air speed in the test section can reach a maximum velocity of 50 m/s. In order to simulate the actual working conditions, ground was constructed using wooden plate. The plate was 4 mm thick, 250 mm wide and with length of 400 mm. The small thickness was used for not to affect the turbulence level of the air free stream. The wooden ground was fixed to the wind tunnel by means of four rods. Two methods of fixation of the model to the wooden ground were used. The first was a total fixation with the ability of changing

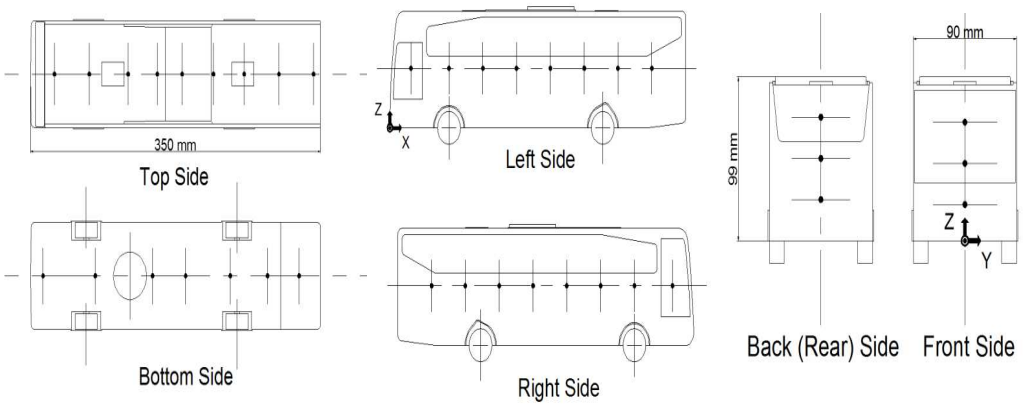

Figure 1 : Schematic drawing of the model showing the positions of origin point and pressure taps.

the yawing angle of the model, while the second method permitted a constrained motion in the free stream direction. Using the first method the pressure distribution and flow visualization of the bus model were possible, while the second method allowed for drag measurement using a force dynamometer.

In order to investigate all the aerodynamic properties of the model, several qualitative and quantitative techniques were carried out. Flow visualization was carried out using two experiments; namely tufts and smoke. In the tufts experiment, woolen threads were fixed along the left, right and top sides of the model; these threads (tufts) show the direction of the flow around the model. The test was filmed by a digital camera of 25 fps. The test was carried out at air velocities of 10, 20 and 30 m/s which correspond to Reynolds number values of 53580, 107160 and 160740 respectively for both yawing and zero yawing positions. In the smoke experiment, a smoke generator was used to generate fine particles of evaporated oil to be injected in the free stream at the center plane of the model. This test was carried out to inspect the boundary layer and the flow behavior at the top of the model. The test was filmed by the same digital camera. The test was carried out at air velocities of 5, 10 and 15 m/s which correspond to Reynolds number values of 26790, 53580 and 80370 respectively at only zero yawing position.

In order to investigate aerodynamic properties quantitatively, pressure along all sides of the model was measured using pressure probes and manometers. Pressure probes were installed at the centerline of each side in the positions shown in figure (1). The manometers used were well-type manometers with 20 legs for each manometer that used water as its fluid. The pressure measurements were carried out at velocities of 10, 15 and 20 m/s which correspond to Reynolds number values of 53580, 80370 and 107160 respectively at both yawing and zero yawing positions. Using these pressure measurements, the pressure coefficients were calculated along all sides of the model from which pressure distributions were obtained. From these pressure distributions, a view of the behavior of the stream flow around the model was deduced for both positions. The lift and drag coefficients were calculated at zero yawing position. Also the drag coefficient was calculated using another method by using a force dynamometer. This method was a more direct way for calculating the drag coefficient

since the actual force was directly measured. Here, the model was connected to the dynamometer by means of a metallic wire. The experiment was carried out at velocities from 5 to 30 m/s at only zero yawing position. All experiments were carried out at Reynolds number values based on the width as the characteristic length of the model.

3. RESULTS AND DISCUSSIONS

3.1 Flow Visualization

Flow visualization experiments were carried out in order to gain qualitative information about the flow behavior around the bus model. In order to do so, two sets of experiments were carried out; the first by using tufts technique and the second by using the smoke.

3.1.1 Tufts experiments

Figure (2) shows the behavior of the flow around the bus at zero yawing position. Figure (2a) shows the flow behavior over the roof of the bus model. From this figure it is clear that a high level of turbulence exists at the leading edge of the roof until x/L = 0.2 which is formed by the vortices existing due to sudden change of the flow from the frontal area of the bus model to flow over the top.

By examining the behavior of the tufts over the bus model roof, it can be found that at its centerline the tufts are in straight formation. This indicates that the flow is directed smoothly in this region from the leading edge towards the trailing edge of the roof. At the side of the roof, the direction of the tufts shows that there is a lateral flow from the centerline towards the sides of the bus model roof but this lateral flow becomes more noticeable at x/L > 0.7.

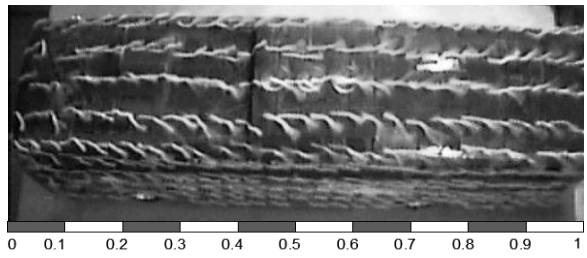

a - Top View

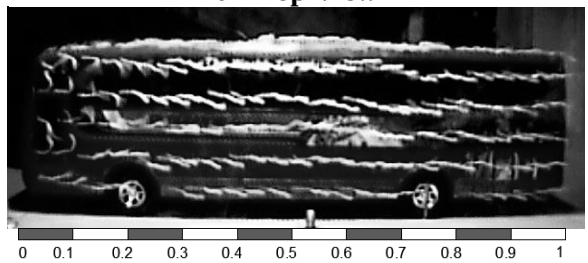

b - Side View

Figure 2 : Tufts tests at zero yaw at Re = 107160.

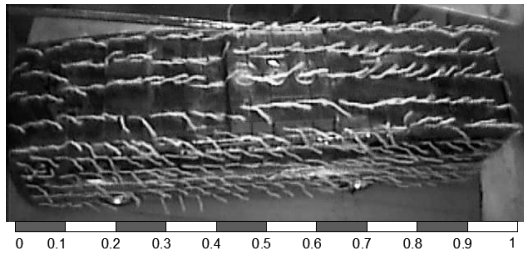

a - Top View

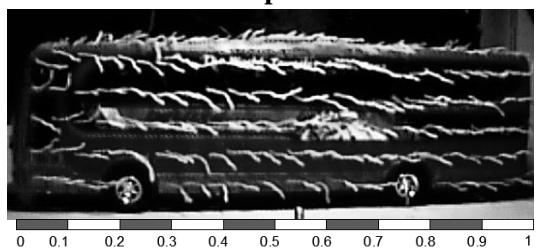

b - Leeward Side

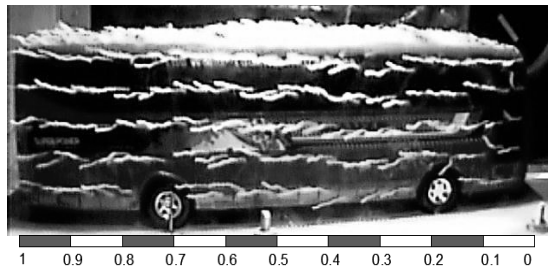

c - Windward Side

Figure 3 : Tufts tests at yawing position at Re = 53580.

Further examination of the side of the bus model, as shown in figure (2b), it is clear that high level of turbulence exists at the leading edge of the side surface until x/L = 0.2 while the direction of the tufts further traveling at the side shows that the air flow is directed from the roof to the sides of the bus towards downward direction which also becomes more noticeable at x/L > 0.7. This will definitely have an impact on the lift forces which will be discussed later.

The flow behavior observed when the bus model was yawed by an angle of 10˚ to the direction of flow is shown in figure (3). Figure (3a) shows the flow behavior over the bus model roof. It indicates high level of turbulence at the leading edge as found before but the flow was directed from the windward side towards the leeward side at the frontal half of the roof. The opposite was found for the back half of the roof. This may be explained by the formation of vortex flow over the bus due to yawing. Figures (3b) and (3c) show the flow at the leeward and windward sides respectively. From these figures it is clear that the flow moves upwards from the windward side over top and then flows downwards at the leeward side. The downward flow in case of yawing is more intense than that in the case with zero yawing.

In both positions, by increasing Reynolds number the same flow pattern is maintained but with increasing turbulence intensity.

3.1.2 Smoke experiments

Figure (4) shows the results of flow visualization using smoke which was carried out at three different values of Reynold numbers. From this figure, it clear that the flow is a stable boundary layer flow from the leading edge of the roof till the step found on the roof where separation occurs and eddies are formed but reattachment of the flow exists near the trailing edge of the roof. This behavior of the flow over the roof of the bus model governs the lift and friction drag characteristics.

a - Re = 53580

b - Re = 80370

c - Re = 107160

Figure 4 : Smoke tests at different values of Reynold numbers.

3.2 Pressure Distribution

The study of pressure distribution over the body of the bus model is important as the pressure distribution data can be analyzed in order to calculate the form drag, lift forces and side forces. The data of pressure distribution over any surface of the bus model is presented using the pressure coefficient (C_p) which is a normalized way of expressing static pressure, [20]. The pressure coefficient is calculated from the following equation:

$$C_p = \frac{P - P_o}{\frac{1}{2}\rho V^2} \quad (1)$$

3.2.1 Pressure distribution at zero yawing position

Figure (5 a to c) compares the pressure coefficient at the front of the bus model to that at the rear side at different values of Reynolds number. From the figure it is clear that for all the examined values of Reynolds number, the pressure coefficient decreases by

increasing the vertical distance away from the origin z/H = 0. This is valid only for the front side of the bus model. At the rear side of the bus model, C_P increases to a maximum value at z/H ≈ 0.5 and then decreases. For the rear side, increasing Reynolds number decreases the pressure coefficients appreciably. This indicates that the increase of Reynolds number increases the vortices behind the bus model leading to the increase of the pressure difference between the front and the back. The latter leads to an increase in the form drag. It is also noticed that the least pressure difference between the front and rear sides is found to occur at z/H ≈ 0.5 for all examined values of Reynolds number.

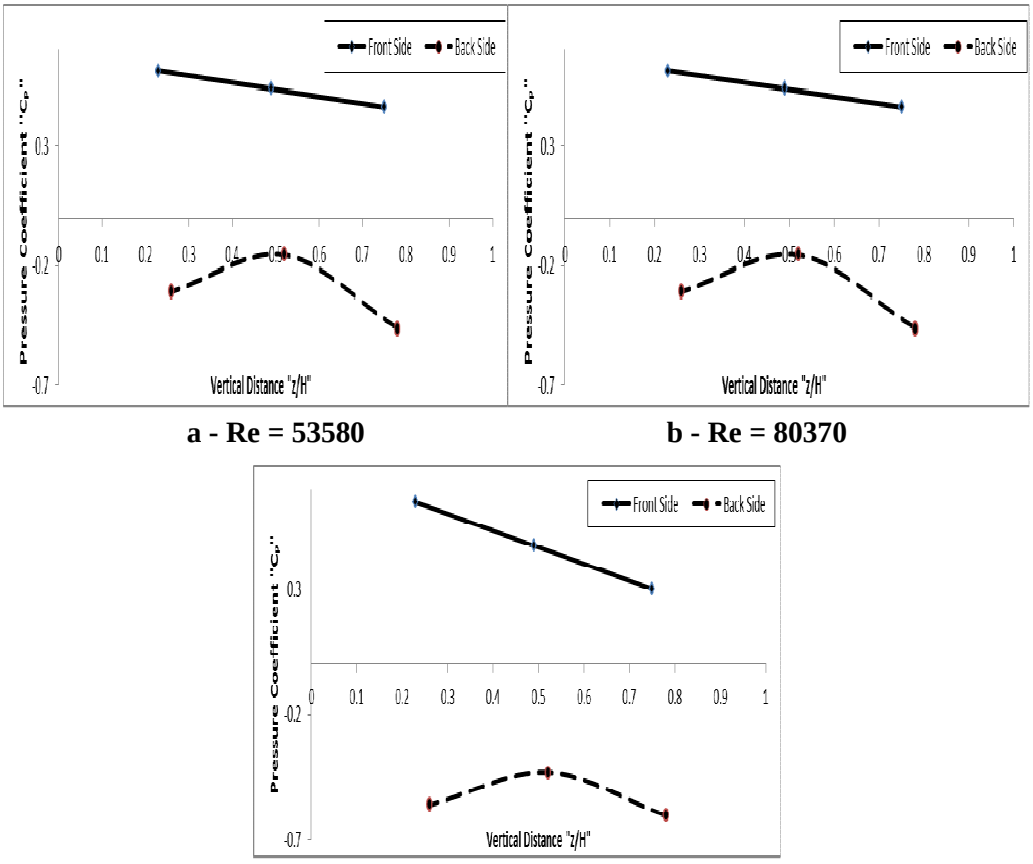

a - Re = 53580 **b - Re = 80370**

c - Re=107160

Figure 5 : Front and back pressure distribution at different values of Reynold Numbers (no yaw).

Figure (6) shows the pressure coefficient measured at the right side of the bus model at zero yaw. Figure (6a) shows that at Re = 53580 the pressure at the leading edge of the side is low then it increases and peaks at x/L = 0.21 then it decreases to a minimum at x/L = 0.41. It peaks again at x/L = 0.54. It decreases to a second minimum at x/L = 0.77 and starts to rise again till the trailing edge of the side. This shows that there is a pressure cycle at the side of the bus model at this Reynolds number. It is to be noted that the pressure in all cases is lower than the reference pressure. When

Reynolds number is raised to 80370 it is noticed from figure (6b) that the pressure coefficient starts with a value very near to that in figure (6a) and peaks at x/L = 0.3 with a value similar to that in figure (6a). For the range of values between 0.44 < x/L < 0.64 the value of the pressure coefficient is nearly constant. For x/L greater than 0.6 it decreases reaching a minimum at x/L = 0.75 and rises again. By raising Reynolds number to 107160 (figure (6c)) a nearly typical curve to that of (6b) but the values of the pressure coefficient are lower except there is no second minimum obtained and the pressure coefficient has low values at the end of the sides. From figure (6) it is clear that changing the air velocity around the bus model affects the pressure distribution along the sides. The values of this pressure are also affected in a way that increasing Reynolds number decreases the pressure at the sides.

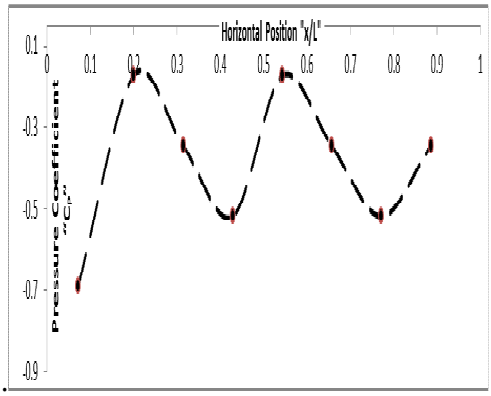

a – Re=53580

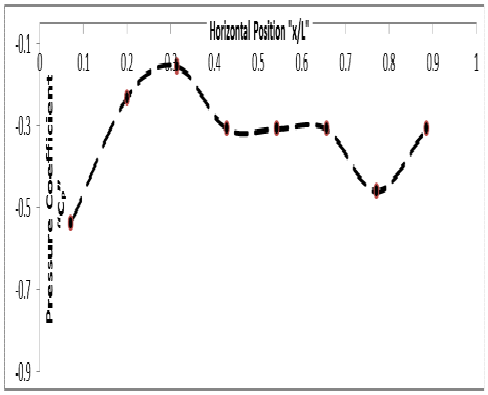

b – Re=80370

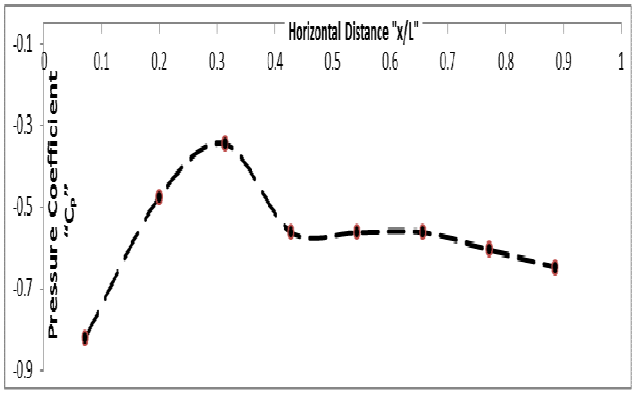

c – Re=107160

Figure 6 : Right side pressure distribution at different values of Reynold Numbers (no yaw).

Figure (7) shows the pressure distribution at the top and the bottom of the bus model at three values of Reynolds number. It is clear from this figure that the coefficient of pressure at the top is generally higher than that at the bottom and the difference between the values of the coefficient of pressure between the top and the bottom decreases by increasing Reynolds number. This difference influences the lift force exerted on the bus during motion. Increasing the flow's Reynolds number the

generated downward force is decreased; i.e. the lift force increase. Also, it is noticed that by increasing Reynolds number the intensity of variation of the pressure coefficient increases. Figure (7a) shows that at Re = 53580 the pressure at the leading edge at the top is high. It then starts to decrease until x/L = 0.34. After that it remains at a nearly constant value until x/L = 0.44 then decreases until x/L = 0.52 and remains constant till x/L = 0.63 after which it decreases till the trailing edge of the bus model. This indicates, generally, that by increasing the distance from the leading edge, the pressure coefficient decreases which is a general trend for all other values of Reynolds number. Figure (7b) shows the variation of pressure coefficient at Reynolds number of 80370. The pressure coefficient at the leading edge at the roof of the bus model is high and decreases to a minimum at x/L = 0.24. It peaks at x/L = 0.44 and a second minimum exists at x/L = 0.63 then reaching a peak at x/L = 0.74 and decreasing till the trailing edge at the top of the bus model. By increasing Reynolds number to 107158 as shown in figure (7c), the same pressure distribution as that of figure (7b) exists but with different values and different positions of peaks and minimums.

For the bottom side of the bus model, for all Reynolds numbers, pressure at the leading edge at the bottom is low then increases till x/L = 0.24. It then generally decreases till the trailing edge as shown in figures (7b) and (7c). This distribution is not

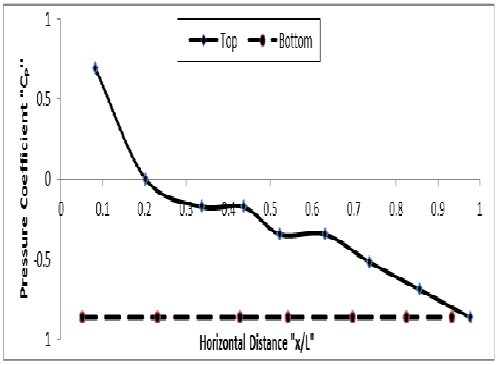

a - Re=53580

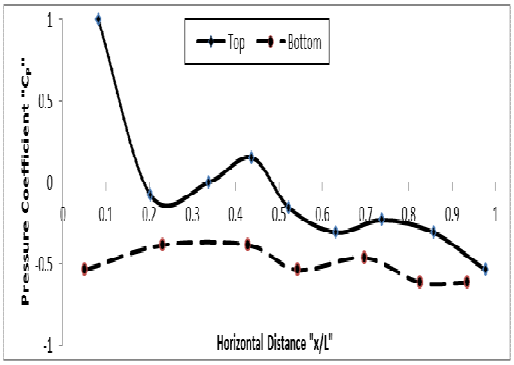

b - Re=80370

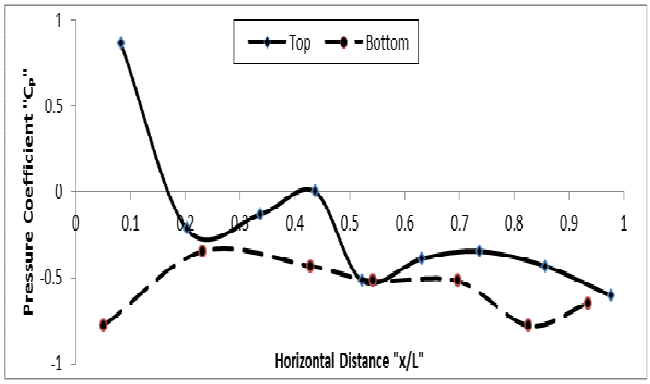

c - Re=107160

Figure 7: Top and bottom pressure distribution at different values of Reynold numbers (no yaw)

maintained at lower values of Reynolds number as in case of Re = 53580 (figure (7a)) for which the pressure coefficient is nearly constant along the bottom side of the bus model. Therefore, it can be concluded that the pressure distribution at the roof of the bus model is more important in the determination of the lift force acting on the bus model than the pressure distribution at the bottom.

3.2.2 Pressure distribution at yawing position

In order to show the effect of crosswind on the bus model at yawing angle 10˚, figure (8) shows the pressure distribution on the sides of the bus model windward and leeward sides. Figure (8a) shows that at Re = 53580 the pressure at the windward side is higher than that at the leeward side. The pressure at the windward side rises from the bus model's leading edge then it reaches a maximum at x/L = 0.25. It then decreases till x/L = 0.43 and afterwards remains constant till the trailing edge of the side of the bus model. The pressure at the leeward side rises from the bus model's leading edge till it reaches a maximum at x/L = 0.32 then remains nearly constant till x/L = 0.52. It then decreases to a minimum to x/L = 0.7 and starts to rise again till the trailing edge. From the previous discussion it is clear that the pressure at the windward side is constant except for the frontal area of the side of the bus model. However for the

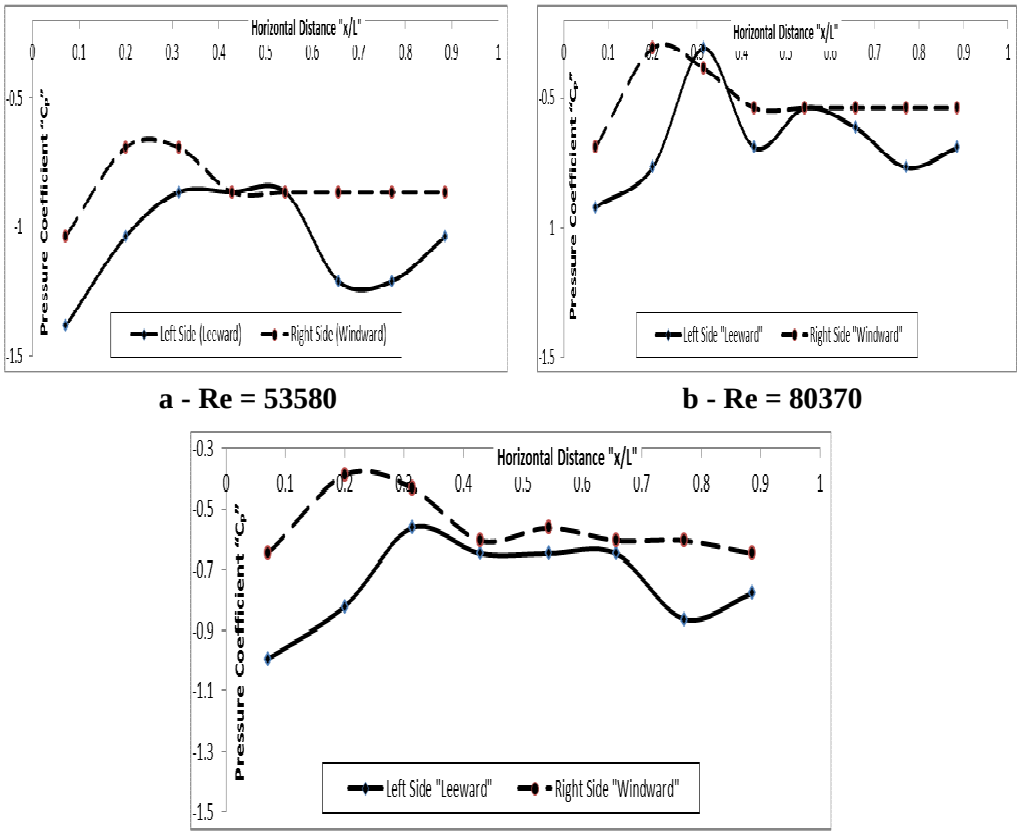

a - Re = 53580 **b - Re = 80370**

c - Re = 107160

Figure 8 : Side pressure distribution at different values of Reynold Numbers (yaw).

leeward side it suffers from change in values. The latter can be explained by the formation of vortices at the leeward side depending on the position at the bus side. Figure (8b) shows the pressure distribution at the side of the bus model at Re = 80370. From this figure it is clear that the trend obtained for the windward side is the same but the pressure values are increased compared to that in figure (8a) and with the peak at x/L = 0.22. Also, the pressure distribution at the leeward side (in figure (8b)) suffers from an oscillation that was not noticed in figure (8a). The pressure at the leading edge is low then the pressure has two peaks at x/L = 0.31 and x/L = 0.55, two minimas at x/L = 0.44 and x/L = 0.78. Figure (8c) shows the pressure distribution of the bus model at Re = 107160, in this case the windward pressures have nearly the same trend as figures (8a) and (8b), but the values are very near to those in figure (8b). For the leeward side, it has similar distribution as that in figure (8b) but with different values except that after the first peak pressure decreases till x/L = 0.43 and remains nearly constant till x/L = 0.64

Therefore, inducing a yaw on the bus model in the flow direction generally affects the pressure distribution at the leeward side more than the windward side and it could be concluded from figure (8) that a side force towards the leeward side exists. This force tends to move the bus model out of its course. Such force increases by increasing Reynolds number, also no yawing moment exists.

Under yawing conditions for the front and back sides, pressure distribution has the same trend as that of a zero yawing position, but the values of the pressure coefficients vary. Despite of varied values, the pressure difference between the front and rear sides is about the same values as in case of zero yawing position. This leads to small differences in form drag force between those positions at a given velocity. Also for the top and bottom sides of the model both the trend and values at yawing position are the same as those at zero yawing position but with negligible differences.

3.3 The Drag and Lift Coefficients

Most of the work carried out to study the aerodynamics of immersed bodies in a fluid focused on calculating drag and lift forces exerted on such bodies. For vehicles as buses, trains and cars, the main concern is to minimize the drag and the lift forces.

In the present work, the drag forces on the bus model were calculated based on pressure distribution measurements and also measurements using force dynamometer. Coefficients were calculated in this work at zero yawing position. It is known that the drag coefficient, hence, the drag force has two components namely they are; friction and form.

Friction drag coefficient (C_{DF}) can be calculated using the following empirical formula for a flat plate, Munson et al. [20];

$$C_{DF} = \frac{0.072}{R_{eL}^{1/5}} \tag{2}$$

In equation (2) Reynolds number "Re_L" is based on the length of the plate (model) turbulent boundary layer is assumed to begin at the leading edge of the surface. Equation (2) treats the friction surfaces of the bus model as separate flat surfaces. The results of this calculation are shown in figure (9). It is clear that by increasing the free stream velocity hence Reynolds number, the coefficient of friction decreases as the

formula implies. Also it is noted that the values of C_{DF} are relatively very low compared with pressure drag coefficient (C_{DP}) at a given Reynolds number.

The form (Pressure) drag coefficient (C_{DP}) can be calculated based on the pressure distribution measured using the following equation:

$$C_{DP} = \frac{\int C_P \cos\theta \, dA}{A} \tag{3}$$

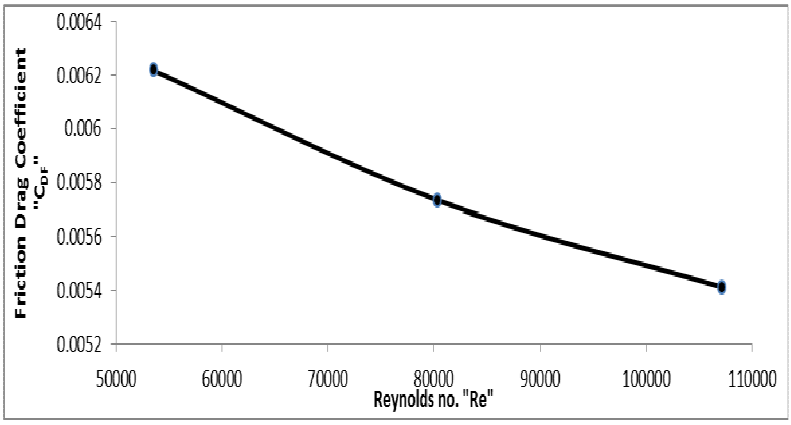

Figure 9 : Variation of friction drag coefficient (C_{DF}) with Reynold's Number.

The results of the form drag are present in figure (10). It is clear that the form drag increases by increasing the flow velocity and hence Reynolds number. Also, C_{DP} is much larger compared to C_{DF} where the contribution of the later to total drag is very low.

Total drag coefficient (C_D) can be calculated by the following formula:

$$C_D = \frac{D_T}{\frac{1}{2}\rho V^2 A} = \frac{AC_{DP} + A_L C_{DF}}{A} \tag{4}$$

The formula given by equation (4), considers the contribution of both pressure and friction drag forces on the total drag force, based on measurements of the total drag force using the dynamometer, D_T is directly measured.

Figure (11) shows the comparison between the drag coefficient calculated from pressure measurements, (C_{DM}), and the drag coefficient using force dynamometer, (C_{DD}). From this figure, it is shown that the calculated values of drag coefficient using pressure measurements are higher than those measured using the force dynamometer. This can be due to an incorrect accounting for the projected area when calculating values of drag coefficient.

It is also clear from figure (11) that the variation of C_{DM} with Reynolds number is similar to that of C_{DP} with Reynolds number. This is because the contribution of friction drag force is very small such that it does not affect the trend of the total drag force. Also the variation of C_{DD} with Reynolds number has some similarity with that of C_{DM}, as it increases with Reynolds number but with different values and slope, which could be due to improper accounting of the frontal area of the bus model.

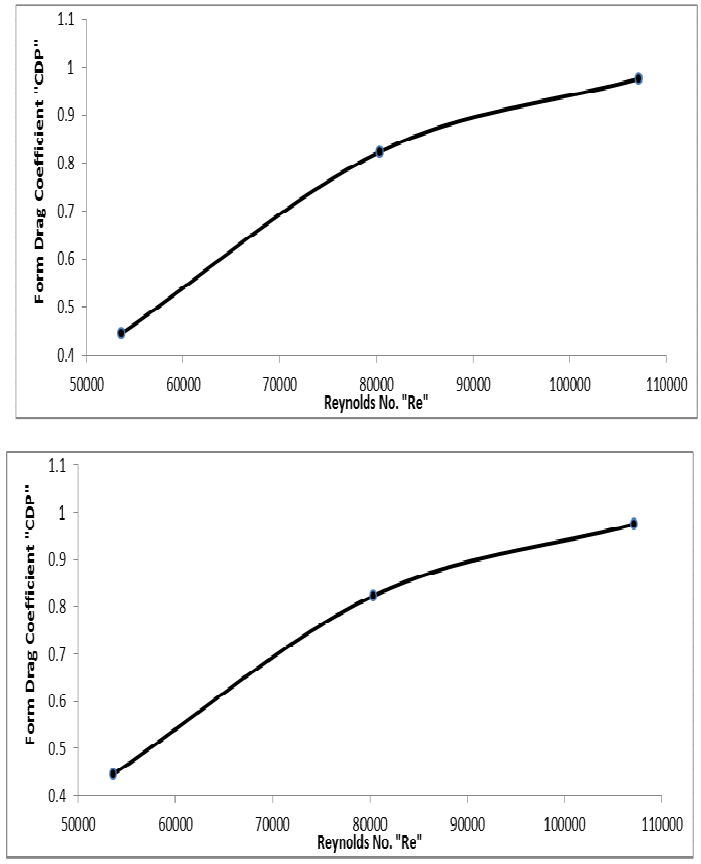

Figure 10 : Variation of form drag coefficient (C_{DP}) with Reynold's Number.

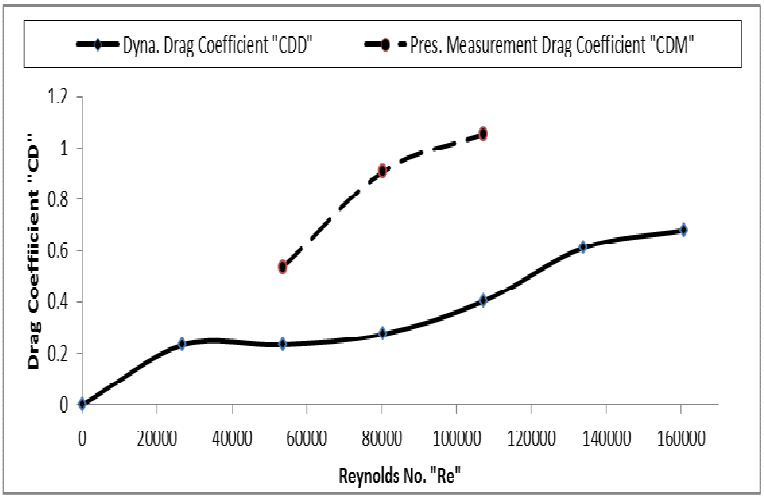

Figure 11 : Variation of total drag coefficient with Reynold's number using force dynamometer (C_{DD}) and pressure measurements (C_{DM}).

The lift coefficient was calculated using the data obtained from the pressure measurements of the top and the bottom sides of the bus model. Lift coefficient (C_L) can be calculated by:

$$C_L = \frac{\int C_p dA}{A_U} \tag{5}$$

Figure (12) show the results of calculating C_L. It is clear that the lift coefficient is negative Hence the total lift force on the model is acting downwards increasing the stability of the bus model. Also increasing the Reynolds number increases the value of the lift coefficient.

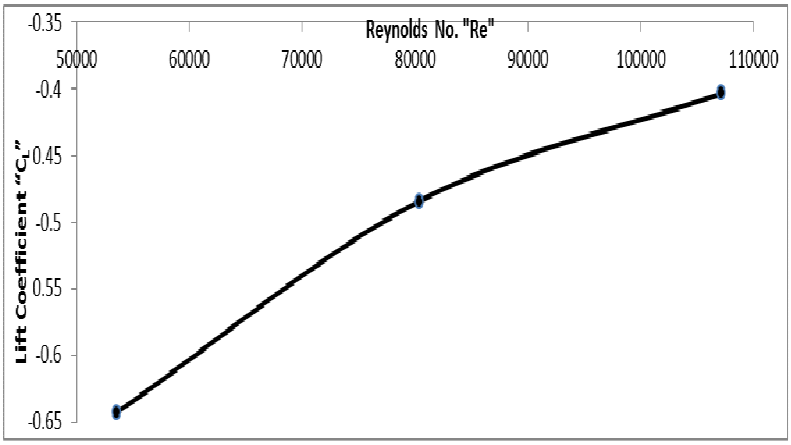

Figure 12 – Variation of lift coefficient (C_L) with Reynold's number.

4. CONCLUSIONS

Based on the present experiments, it was found that the form drag acting on the bus model increases by increasing the air velocity and also that the pressure distribution at the rear of the bus is much more affected by the change in velocity rather than the pressure distribution at the front of the bus model. The coefficient of drag component that mainly dominates the total drag coefficient is the form drag coefficient while the friction drag coefficient has negligible contribution.

The pressure distribution at the sides of the bus in case of zero yaw showed cyclic variation of pressure, but these pressure variations die out by increasing the air velocity.

The lift force on the bus model increases by the increase of the velocity and the pressure distribution at the roof of the bus is greatly affected by the change in velocity compared with the pressure distribution beneath the bus model.

When the bus model was yawed by 10˚, side force exists and its value increases by the increase of velocity. Also it was found that no yawing moment acts on the bus model.

The values of lift and drag coefficients at 10˚ yaw did not vary appreciably from their values at zero yaw.

REFERENCES

[1] Hwang, Jong-Yeon and Yang, Kyung-Soo, 2007. Drag reduction on a circular cylinder using dual detached splitter plates. Journal of Wind Engineering and Industrial Aerodynamics 95, 551-564.

[2] Anderson, E.A.and Szewczyk, A.A., 1997. Effect of a splitter on the near wake of the circular cylinder in 2 and 3 dimensional flow configuration. Exp. Fluids 23, 161-174.

[3] Rathakrishnan, E., 1999. Effect of splitter plate on bluff body drag. AIAA J.37 (9), 1125-1126.

[4] Unal, M.F.and Rockwell, D., 1987. On vortex formation from a cylinder. Part 2. Control by a splitter-plate interference. J. Fluid Mech. 190, 513-529.

[5] Apelt, C.J., West, G.S. and Szewczyk, A., 1973. The effect of wake splitter plates on the flow past a circular cylinder in the range 104 < Re < 5*104. J. Fluid Mech. 61, 187-198.

[6] Kwon, K. and Choi, H., 1995. Control of laminar vortex shedding behind a circular cylinder using splitter plates. Phys. Fluids 8, 479-486.

[7] Hemida, H. and Krajnović, S., 2010. LES study of the influence of the nose shape and yaw angles on the flow structures around trains. Journal of Wind Engineering and Industrial Aerodynamics 98, 34-46.

[8] Cheli, F., Ripamonti, F., Rocchi, D. and Tomasini, G., 2010. Aerodynamic behavior investigation of the new EMUV250 train to cross wind. Journal of Wind Engineering and Industrial Aerodynamics 98, 189-201.

[9] Sterling, M., Quinn, A.D., Hargreaves, D.M., Cheli, F., Sabbioni, E., Tomasini, G., Delaunay, D., Baker, C.J. and Morvan, H., 2010. A comparison of different methods to evaluate the wind induced forces on a high sided lorry. Journal of Wind Engineering and Industrial Aerodynamics 98, 10-20.

[10] Baker, C.J. and Reynolds, S., 1992. Wind-induced accidents of road vehicles. Accident analysis & prevention 24(6), 559-575.

[11] Chiu, T.W., 1995. Prediction of the aerodynamic loads on a railway train in a crosswind at large yaw angles using an integrated two- and three-dimensional source/vortex panel method. Journal of Wind Engineering and Industrial Aerodynamics 57, 19-39.

[12] Chiu, T.W. and Squire, L.C., 1992. An experimental study of the flow over a train in a crosswind at large yaw angles up to 90o. Journal of Wind Engineering and Industrial Aerodynamics 45, 47-74.

[13] Copley, J.M., 1987. The three-dimensional flow around railway trains. Journal of Wind Engineering and Industrial Aerodynamics 26, 21-52.

[14] Suzuki, M., Tanemoto, K. and Maeda, T., 2003.Aerodynamic characteristics of train/vehicles under cross winds. Journal of Wind Engineering and Industrial Aerodynamics 91, 209-218.

[15] Hoppmann, U., Koenig, S., Tielkes, T. and Matschake, G., 2002. A short-term strong wind prediction model for railway application: design and verification. Journal of Wind Engineering and Industrial Aerodynamics 90, 1127-1134.

[16] Ahmed, S.R., Ramm, G. and Faltin, G., 1984. Some salient features of the time-averaged ground vehicle wake. SAE Paper 840300.

[17] Buresti, G., Fedeli, R. and Ferraresi, A., 1997. Influence of afterbody rounding on the pressure drag of an axisymmetrical bluff body. Journal of Wind Engineering and Industrial Aerodynamics 69-71, 179-188.
[18] Prasad and Williamson, C.H.K., 1997. A method for the reduction of bluff body drag. Journal of Wind Engineering and Industrial Aerodynamics 69-71, 155-167.
[19] Allam, A.A., El Rakaybi, A.A., Abdel Nabi, A.A., Al Dahshan, A.G. and Fangary, Y.S., 2010. Pressure Distribution and Flow Visualization of an SUV. Ain Shams Journal of Mechanical Engineering (ASJME), Vol. 2, pp. 181-189.
[20] Munson, B.R., Young, D.P. and Okishi, T.H., 2006, Fundamentals of Fluid Mechanics, fifth edition.

تحليل قوى الديناميكا الهوائية على نموذج لأوتوبيس

قامت أبحاث سابقة بدراسة قوى الديناميكا الهوائية للمركبات الأرضية بغرض التحسين من ثباتها و تحديد القوى الناتجة عن ديناميكا الهواء المؤثرة على تلك المركبات.

الدراسة الحالية ركزت على تأثير القوى الناتجة من ديناميكا الهواء على نموذج لأوتوبيس محاكى للموجود بالواقع. أهتمت الدراسة الحالية بتوزيع ضغط الهواء حول النموذج و قياس قوى الرفع و الجر المؤثرتين على النموذج.

تمت دراسة حالتين: عندما كان النموذج موازيا لاتجاه سريان الهواء و الحالة الأخرى عندما كان النموذج يميل بزاوية مقدارها عشرة درجات مع اتجاه سريان الهواء.